

Magnetic Field-Induced Insulator-Semimetal Transition in a Pyrochlore $\text{Nd}_2\text{Ir}_2\text{O}_7$

K. Ueda,¹ J. Fujioka,¹ B.-J. Yang,² J. Shioyai,³ A. Tsukazaki,³ S. Nakamura,³ S. Awaji,³ N. Nagaosa,^{1,2} and Y. Tokura^{1,2}

¹*Department of Applied Physics and Quantum Phase Electronics Center, University of Tokyo, Tokyo 113-8656, Japan*

²*Center for Emergent Matter Science (CEMS), RIKEN Advanced Science Institute (ASI), Wako 351-0198, Japan*

³*Institute for Materials Research, Tohoku University, Sendai 980-8577, Japan*

(Received 26 February 2015; published 30 July 2015)

We investigate magnetotransport properties in a single crystal of pyrochlore-type $\text{Nd}_2\text{Ir}_2\text{O}_7$. The metallic conduction is observed on the antiferromagnetic domain walls of the all-in–all-out-type Ir $5d$ moment ordered insulating bulk state that can be finely controlled by an external magnetic field along [111]. On the other hand, an applied field along [001] induces the bulk phase transition from insulator to semimetal as a consequence of the field-induced modification of the Nd $4f$ and Ir $5d$ moment configurations. A theoretical calculation consistently describing the experimentally observed features suggests a variety of exotic topological states as functions of electron correlation and Ir $5d$ moment orders, which can be finely tuned by the choice of rare-earth ion and magnetic field, respectively.

DOI: 10.1103/PhysRevLett.115.056402

PACS numbers: 71.30.+h, 72.80.Ga, 75.47.-m, 75.60.-d

Topological electronic states in quantum materials have been subjects of intensive experimental and theoretical studies in condensed matter research [1–6]. Recently, the cooperative effects of electron correlation and spin-orbit coupling have attracted much attention as the central ingredient to synthesize the next-generation topological quantum phase [7]. A Weyl semimetal (WSM) state is one representative example where linearly dispersing bands with the band-crossing Weyl point (WP) show up in a three-dimensional bulk while hosting surface Fermi arc states [8,9], which is proposed to be realized in various correlated magnetic materials [9–17].

Pyrochlore-type $R_2\text{Ir}_2\text{O}_7$ (R —denotes rare-earth, Y, and Bi ion) is one of the promising candidates for the realization of abundant emergent phases including WSM [9,13–20]. The pyrochlore lattice consists of the nested corner-sharing tetrahedra of each R ion and Ir one, as displaced from each other by a half unit cell [Fig. 1(a)] [21]. Owing to large spin-orbit coupling, both R $4f$ and Ir $5d$ spins possess a single-ion magnetic anisotropy denoted by broken lines in the lower panel of Fig. 1(a), which leads to various magnetic ground states [22–26]. For instance, the all-in–all-out (AIAO)-type configuration may be favored with the nearest-neighbor antiferromagnetic exchange coupling where all four spins on the vertices of the pictured tetrahedron point in (4-in–0-out, 4-0) or out (0-in–4-out, 0-4) of its center [23]. Since this ordering pattern breaks time-reversal symmetry while retaining cubic symmetry, the WSM state is predicted to exist with WP at Fermi energy in some parameter regions [13,14,17]. On the other hand, when we apply a magnetic field along the [001] direction ($H\parallel[001]$) and the Zeeman energy overcomes the exchange coupling, two spins point inwards and the other two outwards, forming the so-called 2-in–2-out (2-2) state [26–28]. Such a change of magnetic structure may

reconstruct band structures, which can produce unconventional magnetotransport phenomena [15,29].

The pyrochlore with $R = \text{Nd}$ offers an ideal platform to explore the evolution of an electronic state with the change in magnetic configuration where not only the magnetic moment of Ir $5d$ electrons but also the Nd $4f$ local moment plays a crucial role [14,17]. When it undergoes a metal-insulator transition accompanied by the AIAO-type Ir $5d$ magnetic ordering, Nd $4f$ moments also develop the AIAO-type ordering at lower temperature due to $f-d$ exchange coupling [30–34], although there is not much conclusive evidence about the ordering patterns or different conclusions [35]. Conversely, we may have a chance of largely modifying the Ir $5d$ spin ordering pattern in terms of magnetic-field control of Nd $4f$ moments via the $f-d$ exchange coupling. In fact, characteristic magnetotransport phenomena such as large magnetoresistance are observed in polycrystals, although these origins remain elusive [36,37]. Another remarkable feature of $\text{Nd}_2\text{Ir}_2\text{O}_7$ is an anomalous metallic state on the AIAO-type magnetic domain walls (DWs) contrary to the gapped bulk state [31,38]. These facts indicate that the electronic state strongly couples to the magnetic features in this material, and the study on field-direction-dependent magnetotransport in $R = \text{Nd}$ single crystals is indispensable.

In this Letter, we have investigated the magnetotransport properties with a field-tuned magnetic structure in an $R = \text{Nd}$ single crystal. AIAO-type magnetic DWs hosting metallic states, which clearly show up in the hysteresis both in resistivity and magnetization, can be finely controlled by $H\parallel[111]$. In contrast, the insulating state turns into a semimetallic one under $H\parallel[001]$ where the magnetic structure of the Nd $4f$ moment is in the 2-in–2-out configuration. Combined with our mean-field calculation, we suggest that the observed phase transition can be

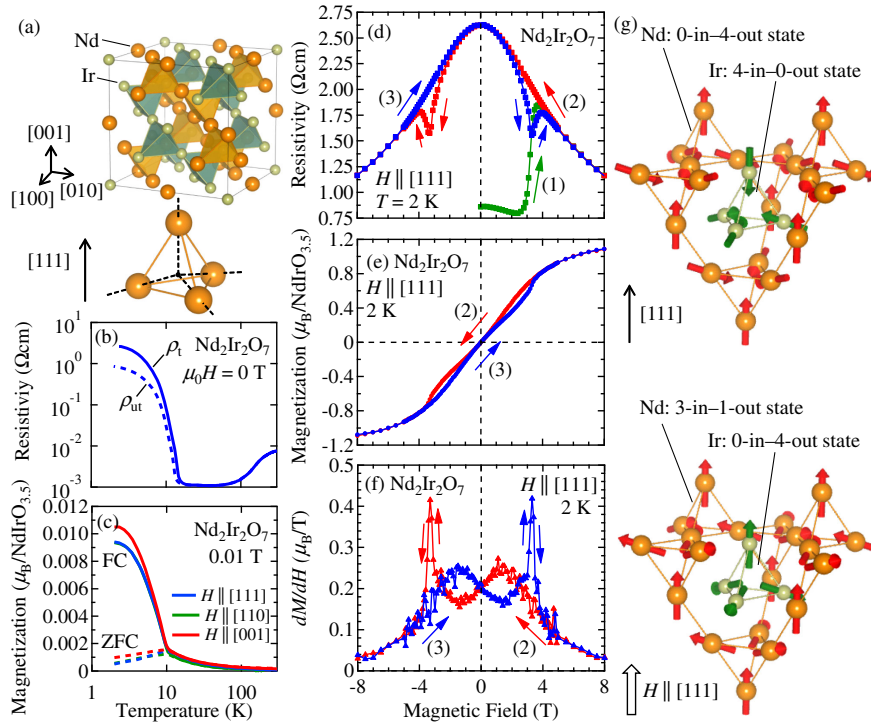


FIG. 1 (color online). (a) Schematic of the Nd₂Ir₂O₇ unit cell and one tetrahedron composed of four ions. The broken lines in the tetrahedron denote the magnetic easy axes. Temperature dependence of (b) the resistivity of the untrained state ρ_{ut} and that of the trained state ρ_t and (c) magnetization in ZFC and FC. Magnetic field dependence of (d) resistivity, (e) magnetization, and (f) field derivative of magnetization for $H \parallel [111]$. The green curve denotes the virgin curve, the red one denotes the sweeping process (2), and the blue one denotes the process (3), respectively. (g) Schematic of the possible magnetic structures in Nd $4f$ moments (red arrows) and Ir $5d$ moments (green arrows). Top figure shows the configuration in the low field, and the bottom figure shows it in a sufficiently strong field along $[111]$.

attributed to the topologically nontrivial band reconstruction with the variation of magnetic structures.

High-quality single-crystalline samples of $R = \text{Nd}$ were synthesized by the KF flux method described in Ref. [39]. We polished the present crystal into a well-formed bar shape. Its dimensions are about $0.75 \times 0.65 \times 0.30 \text{ mm}^3$, suitable for a precise transport measurement. A standard four-probe method was employed for the resistivity measurements with an electric current along the $[1\bar{1}0]$ crystalline axis perpendicular to an applied magnetic field. The resistivity is measured down to 2 K and up to 14 T by using Physical Property Measurement System (Quantum Design). An ac resistance measurement up to 25 T at 27 mK was performed at 1 kHz with an excitation current of 100 μA by using a dilution refrigerator embedded in the cryogen-free hybrid magnet at High Field Laboratory for Superconducting Materials in Institute of Materials Research, Tohoku University [40].

We show the temperature dependence of resistivity and magnetization in Figs. 1(b) and 1(c), respectively. The resistivity in the zero field sharply increases with decreasing temperature below 15 K ($=T_N$), at which the magnetization in zero-field cooling (ZFC) starts to deviate from that in field cooling (FC) pointing to the onset of the AIAO-type magnetic ordering of the Ir $5d$ moment. These anomalies are similar to the data for polycrystalline samples and can be attributed to the AIAO-type magnetic ordering of the Ir $5d$ moment [30,31]. The resistivity in the domain-aligned state (termed trained state, ρ_t) is larger than that in the multidomain state (untrained state, ρ_{ut}), indicating the presence of the metallic DW in the multidomain state, as observed in polycrystals [38].

To quantify the relation between the alignment of the magnetic domain and resistivity in more detail, we show the magnetic field dependence of resistivity and magnetization at 2 K under $H \parallel [111]$ in Figs. 1(d)–1(f). The initial value of resistivity is as small as $\sim 0.8 \text{ } \Omega\text{cm}$ and shows an irreversible jump around +3.4 T on process (1) in Fig. 1(d) due to the field elimination of DWs. With the decreasing field from +14 T [process (2)], the resistivity monotonically increases, reaches the maximum around 0 T, and then the resistivity decreases with a characteristic dip around -3.4 T . The resistivity with the increasing field [process (3)] shows a similar profile to that in process (2), with a dip around +3.4 T. Such hysteresis of magnetoresistivity may be attributed to the transient multidomain state upon the magnetic domain flipping between the 4-0 and 0-4 configuration driven by $H \parallel [111]$ as predicted in Ref. [41] and experimentally demonstrated in Ref. [42]. Another sign of the domain flip is observed in the magnetization as shown in Fig. 1(e). It monotonically increases as a function of the field and saturates in a high magnetic field around $\sim 1.2 \text{ } \mu_B/\text{NdIr}_{0.35}$. Since the magnitude of the magnetization is nearly governed by the Nd $4f$ moment ($\sim 2.37 \text{ } \mu_B/\text{mol}$ [32]) rather than the Ir $5d$ moment ($\sim 0.2 \text{ } \mu_B/\text{mol}$ [32,43]), it is anticipated that the magnetic structure of the Nd sublattice gradually turns into a three-in-one-out (3-1) configuration from a 0-4 one at zero field so as to reconcile with the Zeeman energy, as frequently observed in pyrochlore oxides [26–28]. We note that the magnetization shows a small hysteresis below 4 T and tiny kinks at $\pm 3.4 \text{ T}$, as also reported in Refs. [37,38]. These are more clearly identified in the profile of dM/dH shown in Fig. 1(f). It clearly exhibits a peak at +3.4 T (-3.4 T) in process (2) [process (3)], which corresponds to the kink in

magnetization. These observed properties provide insights about the magnetic structure under $H \parallel [111]$ as depicted in Fig. 1(g). In low fields, the Nd 4*f* moment forms a 0-4 configuration stabilizing the Ir 5*d* 4-0 state, as depicted in the top figure of Fig. 1(g). As the field increases, the Nd 4*f* moment may gradually turn into a 3-1 state due to the competition between Zeeman energy and exchange coupling. Such modulations of the Nd sublattice can flip the 4-0 magnetic domain of the Ir sublattice to a 0-4 one through the *f*–*d* exchange coupling as shown in the bottom of Fig. 1(g).

Figure 2 shows the field dependence of resistivity and magnetization at 2 K for $H \parallel [111]$, $[110]$, and $[001]$, respectively. The negative magnetoresistance is observed for all field directions [44]. Remarkably, the resistivity for $H \parallel [001]$ decreases by 3 orders of magnitude at 14 T and shows a clear hysteresis between the increasing and decreasing field processes above 8 T. The inset of Fig. 2(a) shows the result of the $H \parallel [001]$ scan up to above 20 T at 27 mK. The resistivity saturates and reaches the minimum of ~ 1.6 m Ω cm closing the hysteresis curve above 15 T, reminiscent of the first-order insulator-semimetal transition induced by a magnetic field in colossal magnetoresistance manganites [45]. The magnetization for $H \parallel [001]$ monotonically increases as the field increases, saturating in the high

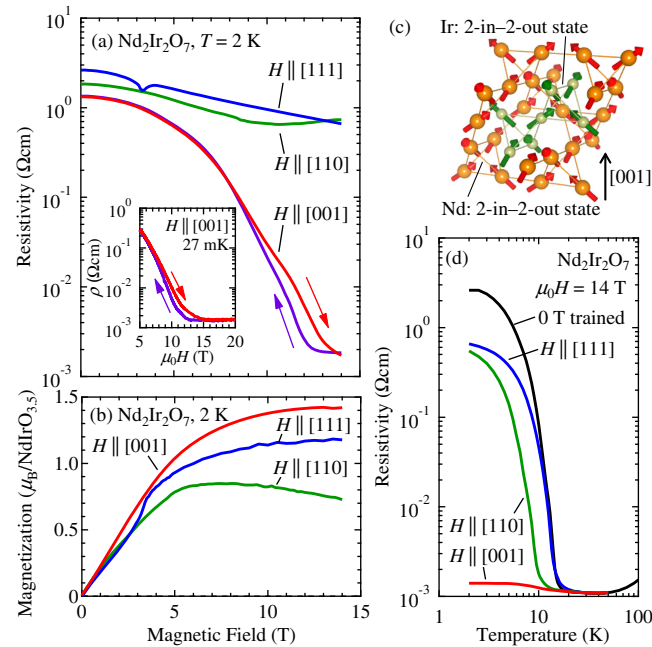


FIG. 2 (color online). Magnetic field dependence of the (a) resistivity and (b) magnetization at 2 K for several field directions. The blue curve denotes $H \parallel [111]$, the green one $H \parallel [110]$, and the red (purple) one $H \parallel [001]$ on the increasing (decreasing) field processes, respectively. The inset to (a) shows the field dependence of the resistivity for $H \parallel [001]$ up to 20 T at 27 mK. (c) Schematic of the possible spin configurations in $H \parallel [001]$. (d) Temperature dependence of ρ_t (black line), $\rho(14$ T) along $H \parallel [111]$ (blue line), $H \parallel [110]$ (green line), and $H \parallel [001]$ (red line), respectively.

field up to $\sim 1.4\mu_B/\text{NdIrO}_{3.5}$, ensuring the formation of the Nd 4*f* moment 2-2 configuration [26–28]. The 2-2-type Nd 4*f* configuration may turn the AIAO-type Ir 5*d* configuration into the 2-2-type one via *f*–*d* exchange interaction as illustrated in Fig. 2(c); this is likely the origin of the observed insulator-semimetal transition. Moreover, as shown in Fig. 2(d), the field along the $[001]$ direction nearly smears out the upturn of resistivity upon the semimetal-insulator transition with lowering temperature, whereas the resistivity increases rapidly below T_N in other field directions.

To confirm the electronic band structure reconstruction driven by the change in magnetic orders, we have investigated the field-angular dependence of the resistivity in Fig. 3. Prior to the measurements, we apply $H \parallel [111]$ to realize the 4-0 single-domain state. The origin of the rotation angle ($\theta = 0^\circ$) is defined to be the $H \parallel [111]$ direction, and the field is rotated around the $[1\bar{1}0]$ axis parallel to the current direction (see the lower left inset of Fig. 3), passing through along the $[110]$ axis at $\theta = 35^\circ$, the $[00\bar{1}]$ axis at $\theta = 125^\circ$, and finally reaches the $[\bar{1}\bar{1}\bar{1}]$ axis at $\theta = 180^\circ$. The right lower inset of Fig. 3 shows the magnified figure of conductivity (inverse of resistivity) on a linear scale. The peak structure appears right above $\theta = 35^\circ$ at 14 T, shifts to a larger angle position with decreasing field, and suddenly disappears below 3 T. The magnitude of the conductivity peak observed above 4 T is almost independent of the field amplitude. Moreover, around $\theta = 125^\circ$, significant reductions of resistivity are observed, and its magnitude strongly depends on the strength of the magnetic field. Similar behavior is identified in the region of 180° – 360° , suggesting the 180° periodicity. The

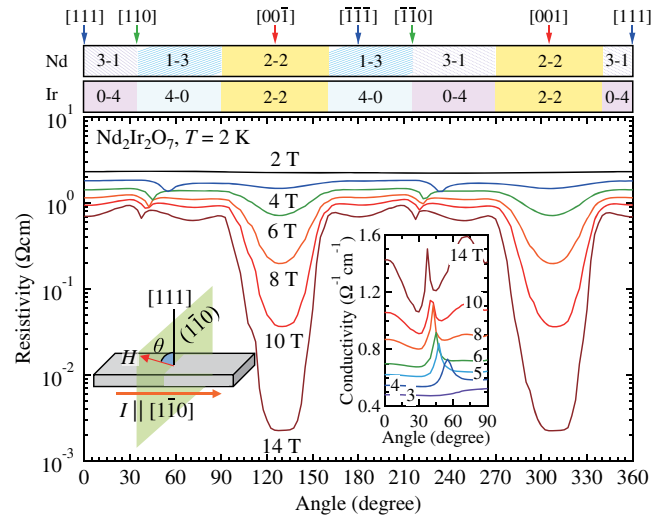


FIG. 3 (color online). The two top tables denote the possible magnetic structures of the Nd 4*f* and Ir 5*d* moments in the strong field limit. The numbers denote the magnetic moment configurations as described in the text. The bottom figure shows the angle dependence of resistivity (on a logarithmic scale) for several fields. The left inset exhibits the experimental configuration. The right inset shows the low angle dependence of conductivity (on a linear scale) for several fields.

conductivity peak (resistivity dip) structure around $\theta = 35^\circ$ is clearly attributed to the flipping of the Ir 5d moment between the 4-0 and 0-4 configuration which accompanies the proliferation of metallic DW, since $\theta = 35^\circ$ is the boundary between the different Nd 4f moment textures of the 1-3 and 3-1 patterns in the high-field limit as shown in the top label of Fig. 3. Another remarkable feature is the reduction of resistivity in the range of 90° – 160° , where the 2-2 state can be favored in the strong field limit. Such a sudden decrease of resistivity cannot be explained in terms of conventional angle-dependent resistivity in the fixed band structure or of scattering by magnetic impurities, rather pointing to the field-induced electronic-structure modulation coupled to the 2-2 magnetic structure.

To elucidate the role of the $f-d$ exchange coupling and electron correlation in $R = \text{Nd}$, we have performed a self-consistent mean-field study of an extended Hubbard model [13,14], the details of which are given in the Supplemental Material [46]. Let us first consider the case of $H\parallel[111]$. Because of Zeeman energy, the Nd 4f configuration evolves from 0-4 to 3-1 as H increases. Accordingly, the effective magnetic field (h_{eff}) induced by $f-d$ exchange coupling forces the Ir 5d configuration to change from 4-0 to 0-4 as described in Fig. 4(a). Since both U and h_{eff} favor the 4-0 or 0-4 configuration, they work cooperatively [14]. Namely, the critical value of U (U_c) for the WSM-insulator transition becomes smaller as h_{eff} gets larger. The field-induced variation of h_{eff} is described by using a parameter $x \in [0, 1]$. Here, $x = 0$ ($x = 1$) indicates the case when the Nd sublattice forms a 0-4 (3-1) configuration uniformly through the sample in the small (large) H limit. The range of $0 < x < 1$ describes the continuous evolution of the Nd 4f configuration between these two limits ($x = M/M^{\text{sat}}$). Since $h_{\text{eff}}(x = 0)$ and $h_{\text{eff}}(x = 1)$ have the opposite sign, it should vanish at a certain point $x_c \in (0, 1)$. In fact, this is the point ($x_c = 0.6$) where U_c is at maximum in Fig. 4(e). Since both the WSM and the insulator have zero density of states on the Fermi level [$D(E_F) = 0$], the magnetotransport would not show an abrupt change as H varies, being consistent with the experiment. Although Zeeman coupling of Ir 5d electrons can induce small electron-hole pockets in WSM due to broken cubic symmetry, the Zeeman energy scale is so tiny that its contribution to transport is negligible [46]. On the other hand, when $H\parallel[001]$, the Nd sublattice develops the 2-2 configuration to induce the 2-2 Ir 5d state via $f-d$ coupling in the large H limit. It is worth to note that the 2-2 Ir 5d state has a completely different nature as compared to the AIAO one which is basically a WSM having eight WPs on the Fermi level [Fig. 4(c)]. When $U < U_c$, the ground state of the 2-2 Ir 5d configuration is a nodal semimetal [10,11,47] [SM* in Fig. 4(f)] with a line node on the $k_z = 0$ plane and two WPs on the k_z axis [Fig. 4(d)]. Since the states on the line node are not degenerate, small electron or hole pockets appear on the $k_z = 0$ plane. Similarly, two WPs on the k_z axis develop small electron pockets. However, since the size of these

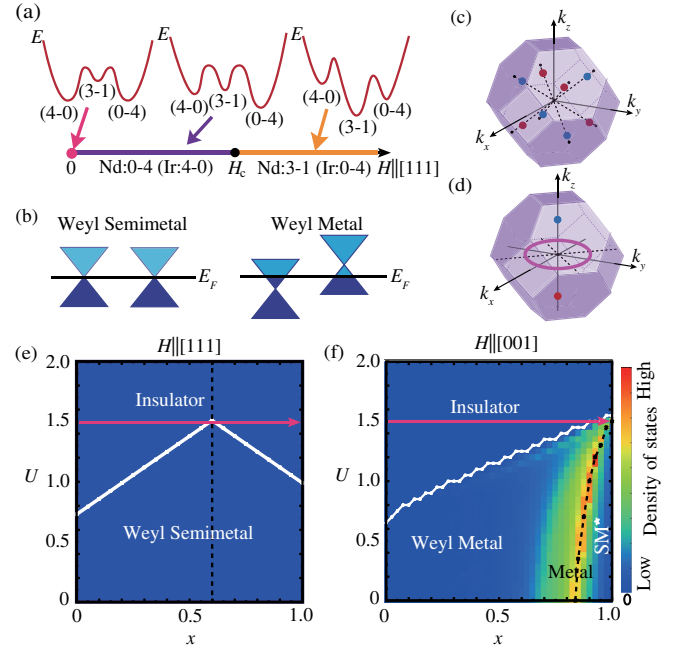


FIG. 4 (color online). (a) Schematic of the free energy E as a function of $H\parallel[111]$. (b) Schematic band structures near Fermi energy E_F for WSM and WM. Distribution of nodal points in the momentum space for the (c) WSM state with an AIAO Ir 5d magnetic pattern and (d) nodal semimetal (SM*) with the 2-2 one. A red (blue) dot indicates a Weyl point with the chiral charge $+1$ (-1), and the purple ring denotes a line node. Electronic phase diagram based on a mean-field theory for (e) $H\parallel[111]$ and (f) $H\parallel[001]$, respectively. The horizontal axis (x) denotes the continuous evolution of the Nd 4f spin configuration from the 0-4 to 3-1 states in (e) and from 0-4 to 2-2 in (f). The red arrow indicates the evolution of the system as H increases, which can consistently describe the magnetotransport observed in experiment.

electron or hole pockets is so tiny, $D(E_F)$ is still very small. Such a huge difference in the nature of the Fermi surface topology between the 2-2 and AIAO Ir 5d states gives rise to intriguing magnetotransport properties of the system. For small H (or small x) where the 4-0 Ir 5d configuration dominates over the 2-2 one, the phase diagram is basically similar to the case of $H\parallel[111]$. However, since the small 2-2 Ir 5d component breaks the cubic symmetry, the WSM turns into a WM with small electron or hole pockets and, hence, $D(E_F)$ becomes nonzero. As H (or x) grows, we can see a sharp increase of $D(E_F)$ in a small window. In fact, this is the region where the Fermi surface topology changes. The distortion of the band structure to mediate two topologically distinct semimetals WM and SM* induces a huge $D(E_F)$ as shown in Fig. 4(f), which is assigned to the physical origin of the observed metallic behavior when $H\parallel[001]$. The theoretical calculation with $U_c \sim 1.5$ (in the unit of electron hopping interaction) appears to well account for the observed properties as shown in the red arrows in Figs. 4(e) and 4(f).

In conclusion, we have presented the magnetotransport properties upon the magnetic field modulation of a magnetic structure in an $R = \text{Nd}$ single crystal. $H\parallel[111]$ can align the

AIAO-type single-domain state and switch two variants to each other, leading to the characteristic hysteresis in resistivity and magnetization. In contrast, $H\parallel[001]$ turns the insulating phase with AIAO magnetic structure into the unconventional semimetallic phase with a 2-2 state. The theoretical calculation suggests that the magnetic field-induced switching of Nd $4f$ spin configurations from the AIAO to the 2-2 state modifies the topological nature of the Ir $5d$ band structure, which can account for the unconventional magnetotransport properties.

We are grateful to T. Kurumaji, Y. Yamaji, and M. Imada for fruitful discussions. This work is supported by the Japan Society for the Promotion of Science through the Funding Program for World-Leading Innovative R&D on Science and Technology (FIRST Program) on “Quantum Science on Strong Correlation” initiated by the Council for Science and Technology Policy, and by the JSPS Grant-in-Aid for Scientific Research (Grants No. 80609488 and No. 24224009).

-
- [1] M. Z. Hasan and C. L. Kane, *Rev. Mod. Phys.* **82**, 3045 (2010).
- [2] Z. Wang, Y. Sun, X.-Q. Chen, C. Franchini, G. Xu, H. Weng, X. Dai, and Z. Fang, *Phys. Rev. B* **85**, 195320 (2012).
- [3] Z. K. Liu *et al.*, *Science* **343**, 864 (2014).
- [4] M. Neupane *et al.*, *Nat. Commun.* **5**, 3786 (2014).
- [5] B.-J. Yang and N. Nagaosa, *Nat. Commun.* **5**, 5161 (2014).
- [6] S.-Y. Xu *et al.*, *Science* **347**, 294 (2015).
- [7] W. W.-Krempa, G. Chen, Y. B. Kim, and L. Balents, *Annu. Rev. Condens. Matter Phys.* **5**, 57 (2014).
- [8] S. Murakami, *New J. Phys.* **9**, 356 (2007).
- [9] X. Wan, A. M. Turner, A. Vishwanath, and S. Y. Savrasov, *Phys. Rev. B* **83**, 205101 (2011).
- [10] G. Xu, H. Weng, Z. Wang, X. Dai, and Z. Fang, *Phys. Rev. Lett.* **107**, 186806 (2011).
- [11] C. Fang, M. J. Gilbert, X. Dai, and B. A. Bernevig, *Phys. Rev. Lett.* **108**, 266802 (2012).
- [12] X. Wan, A. Vishwanath, and S. Y. Savrasov, *Phys. Rev. Lett.* **108**, 146601 (2012).
- [13] W. Witczak-Krempa and Y. B. Kim, *Phys. Rev. B* **85**, 045124 (2012).
- [14] G. Chen and M. Hermele, *Phys. Rev. B* **86**, 235129 (2012).
- [15] S.-B. Lee, A. Paramakanti, and Y. B. Kim, *Phys. Rev. Lett.* **111**, 196601 (2013).
- [16] Y. Yamaji and M. Imada, *Phys. Rev. X* **4**, 021035 (2014).
- [17] B.-J. Yang and N. Nagaosa, *Phys. Rev. Lett.* **112**, 246402 (2014).
- [18] D. Pesin and L. Balents, *Nat. Phys.* **6**, 376 (2010).
- [19] B.-J. Yang and Y. B. Kim, *Phys. Rev. B* **82**, 085111 (2010).
- [20] M. Kurita, Y. Yamaji, and M. Imada, *J. Phys. Soc. Jpn.* **80**, 044708 (2011).
- [21] J. S. Gardner, M. J. P. Gingras, and J. E. Greedan, *Rev. Mod. Phys.* **82**, 53 (2010).
- [22] M. J. Harris, S. T. Bramwell, D. F. McMorrow, T. Zeiske, and K. W. Godfrey, *Phys. Rev. Lett.* **79**, 2554 (1997).
- [23] S. T. Bramwell and M. J. Harris, *J. Phys. Condens. Matter* **10**, L215 (1998).
- [24] M. J. Harris, S. T. Bramwell, P. C. W. Holdsworth, and J. D. M. Champion, *Phys. Rev. Lett.* **81**, 4496 (1998).
- [25] S. T. Bramwell and M. J. P. Gingras, *Science* **294**, 1495 (2001).
- [26] H. Fukazawa, R. G. Melko, R. Higashinaka, Y. Maeno, and M. J. P. Gingras, *Phys. Rev. B* **65**, 054410 (2002).
- [27] Y. Taguchi, T. Sasaki, S. Awaji, Y. Iwasa, T. Tayama, T. Sakakibara, S. Iguchi, T. Ito, and Y. Tokura, *Phys. Rev. Lett.* **90**, 257202 (2003).
- [28] Y. Machida, S. Nakatsuji, Y. Maeno, T. Tayama, T. Sakakibara, and S. Onoda, *Phys. Rev. Lett.* **98**, 057203 (2007).
- [29] L. Balicas, S. Nakatsuji, Y. Machida, and S. Onoda, *Phys. Rev. Lett.* **106**, 217204 (2011).
- [30] K. Matsuhira, M. Wakeshima, Y. Hinatsu, and S. Takagi, *J. Phys. Soc. Jpn.* **80**, 094701 (2011).
- [31] K. Ueda, J. Fujioka, Y. Takahashi, T. Suzuki, S. Ishiwata, Y. Taguchi, and Y. Tokura, *Phys. Rev. Lett.* **109**, 136402 (2012).
- [32] K. Tomiyasu, K. Matsuhira, K. Iwasa, M. Watahiki, S. Takagi, M. Wakeshima, Y. Hinatsu, M. Yokoyama, K. Ohoyama, and K. Yamada, *J. Phys. Soc. Jpn.* **81**, 034709 (2012).
- [33] H. Sagayama, D. Uematsu, T. Arima, K. Sugimoto, J. J. Ishikawa, E. O’Farrell, and S. Nakatsuji, *Phys. Rev. B* **87**, 100403 (2013).
- [34] H. Guo, K. Matsuhira, I. Kawasaki, M. Wakeshima, Y. Hinatsu, I. Watanabe, and Z.-a. Xu, *Phys. Rev. B* **88**, 060411 (2013).
- [35] S. M. Disseler, C. Dhital, T. C. Hogan, A. Amato, S. R. Giblin, C. de la Cruz, A. Daoud-Aladine, S. D. Wilson, and M. J. Graf, *Phys. Rev. B* **85**, 174441 (2012); S. M. Disseler, *Phys. Rev. B* **89**, 140413 (2014).
- [36] K. Matsuhira, M. Tokunaga, M. Wakeshima, Y. Hinatsu, and S. Takagi, *J. Phys. Soc. Jpn.* **82**, 023706 (2013).
- [37] S. M. Disseler, S. R. Giblin, Chetan Dhital, K. C. Lukas, Stephen D. Wilson, and M. J. Graf, *Phys. Rev. B* **87**, 060403 (2013).
- [38] K. Ueda, J. Fujioka, Y. Takahashi, T. Suzuki, S. Ishiwata, Y. Taguchi, M. Kawasaki, and Y. Tokura, *Phys. Rev. B* **89**, 075127 (2014).
- [39] J. N. Millican, R. T. Macaluso, S. Nakatsuji, Y. Machida, Y. Maeno, and J. Y. Chan, *Mater. Res. Bull.* **42**, 928 (2007).
- [40] K. Watanabe, G. Nishijima, S. Awaji, K. Takahashi, K. Koyama, N. Kobayashi, M. Ishizuka, T. Itou, T. Tsurudome, and J. Sakuraba, *IEEE Trans. Appl. Supercond.* **16**, 934 (2006).
- [41] T. Arima, *J. Phys. Soc. Jpn.* **82**, 013705 (2013).
- [42] S. Tardif, S. Takeshita, H. Ohsumi, J.-i. Yamaura, D. Okuyama, Z. Hiroi, M. Takata, and T.-h. Arima, *Phys. Rev. Lett.* **114**, 147205 (2015).
- [43] M. C. Shapiro, S. C. Riggs, M. B. Stone, C. R. de la Cruz, S. Chi, A. A. Podlesnyak, and I. R. Fisher, *Phys. Rev. B* **85**, 214434 (2012).
- [44] The decrease of magnetization is discerned in the high-field region for $H\parallel[110]$; this might be due to the strong diamagnetism arising from the interband orbital effect as frequently observed in a narrow-gapped or gapless system, since $H\parallel[110]$ can hardly modify the AIAO configuration of Ir $5d$ moments.
- [45] H. Kuwahara, Y. Tomioka, Y. Moritomo, A. Asamitsu, M. Kasai, R. Kumai, and Y. Tokura, *Science* **272**, 80 (1996).
- [46] See the Supplemental Material at <http://link.aps.org/supplemental/10.1103/PhysRevLett.115.056402> for details about the model and calculation.
- [47] A. A. Burkov, M. D. Hook, and L. Balents, *Phys. Rev. B* **84**, 235126 (2011).